OPTIMIZED NODALIZATION OF A REACTOR CORE MODEL FOR REAL TIME SIMULATION APPLICATIONS

A Thesis

Submitted to the Graduate Faculty of the
Louisiana State University and
Agricultural and Mechanical College
in partial fulfillment of the
requirements for the degree of
Master of Science in
Nuclear Engineering

in

The Nuclear Science Center

by
Charles A. Rohrmann
B.S., Louisiana State University, 1989
December 1994

TABLE OF CONTENTS

LIST OF TABLES

LIST OF FIGURES

ABSTRACT

Nuclear power plant simulators used for operator training represent a compromise between system modeling detail and cost. Although the reactor core model in the simulator software can vary in detail from a single calculational node to as many as 2500 nodes, the power plant operator typically has indication of neutron flux level at only 100-150 core locations. In this research work, a comparison of a single core model with nodalization varied from approximately one node for every three nuclear instrumentation locations to approximately ten nodes for every nuclear instrumentation location is performed in response to a boiling water reactor control rod drop accident. The comparison indicates that sharper detail is obtained at the highest level of nodalization; however the case where approximately two core nodes are modeled for each nuclear instrumentation location provides a good compromise with acceptable performance for use in real time simulation applications.

INTRODUCTION

The use of simulators for training of technical personnel dates back to World War II with the Link Trainer aircraft simulator. The demand for aircraft on the front lines meant that few aircraft were available for use in pilot training. But it was obvious that time at the controls was necessary if new pilots were to be effective. The Link Trainer permitted fundamental skills training without the actual use of aircraft. This allowed more efficient use of actual flying time since the basic skills had already been mastered on the ground.

The use of simulators in the training of commercial nuclear power plant operators developed along similar lines. The military nuclear power programs originally utilized prototype reactors to train operators. However, commercial power plants cannot afford the luxury of cycling their plants up and down to train new operators. The first attempt at satisfying the need for "at the controls" training was made by the reactor vendors. General Electric built the first nuclear power plant simulator in the late 1960's based on the Dresden-2 plant. The Dresden simulator was located in the General Electric Training Center in Morris, Illinois. General Electric used the simulator to train operators for their customers' boiling water reactor plants. That simulator was followed by three other

simulators. Babcock & Wilcox bought their simulator based on the Rancho Seco plant from the Singer-Link Company. Westinghouse and Combustion Engineering developed their own simulators based on the Zion-1 and Calvert Cliffs plants respectively. All four simulators were in service by 1973 (Gonsalves and Procter 1987).

The available computer systems in the 1970's were relatively expensive and had minimal capacity. This required a number of compromises in modeling of the plant components and systems. The reactor core models were very compact and simple by necessity.

Eight additional simulators were built during the next six years from 1974 to 1979. But in 1979 an event occurred that turned a sideline business of constructing nuclear power plant simulators into a booming opportunity. The accident at the Three Mile Island power plant emphatically demonstrated the need for better operator training. The U.S. Congress directed the U.S. Nuclear Regulatory Commission (NRC) to promulgate regulations requiring the use of plant specific simulators in the training and examination of licensed operators. Over the next ten years orders were placed for close to 100 additional simulators.

The available computer technology advanced rapidly during this period of time. This permitted utilization of considerably more detailed system models than contained in the original reactor vendor simulators. Core models

advanced from as few as a single calculational node to as many as 150 nodes. The simulator vendors were able to perform benchmark comparisons against the performance of much more detailed design computer codes with very good results.

The continued advancements in computing power permitted the simulation business to shift from the production of full scope simulators to the development and installation of advanced models. This shift was necessary for the survival of a domestic simulation industry since all of the operating U.S. nuclear power plants had already taken delivery of their simulators by 1993. In theory, simulator development could be a sustaining business since it is always possible to model a system or component in more detail for greater accuracy, or to extend the simulator model to address more degraded plant conditions.

In practice, there are both physical and financial limits to what utility companies will spend to enhance their simulation models. Modifications to simulation models are generally undertaken in response to regulatory pressure. Competition between simulation vendors has generally been centered around variation in the degree of model accuracy. Utility companies must evaluate the benefits of an enhanced model against the cost of that model.

The objective of this research is to provide some insight into advanced reactor core models for power plant simulators. The simulation services vendors offer core models with varying levels of nodalization. The constraint that these models must run in real time and the nodalization utilized by the fuel vendor or utility core analysis group set an upper limit in the number of nodes at around 5000 - 10,000. The current offerings by the simulation vendors vary from 150 nodes to 2500 nodes.

Core safety analysis-grade computer codes use very fine nodalization to accurately predict the local fuel temperature and other variables for a range of transients encountered in various accident scenarios. By comparison, simulation codes only need to provide the behavior of the simulated nuclear instrumentation system that is observed by the reactor operator. Instead of being concerned with the time-dependant neutron flux level at 5000 - 10,000 points within the core, simulators only require the flux level at 100 - 200 points. Hence it would appear that a much lower level of nodalization should be acceptable in simulators as compared to safety analysis codes. The objective of this research is to provide a comparison of the nuclear instrumentation system response for varying levels of core nodalization.

METHOD OF ANALYSIS

The method used to compare levels of nodalization in simulation core models was to select one particular analysis code and vary the level of nodalization for that code. A specific transient was selected as a reference to judge the performance of the code.

The computer code selected was a proprietary code from one of the simulation vendors. This code is used in over 30 simulators in the U.S. at nodalization levels of 150 to 450 nodes. The code is based on the FLARE code developed for the Atomic Energy Commission in 1964 (Delp et al. 1964).

The code was delivered utilizing 150 nodes to model the River Bend Station fuel cycle 4 core. The River Bend Station is a General Electric version 6 boiling water reactor (BWR-6) with 624 fuel assemblies and 132 in-core fission chambers utilized to determine both local and average neutron flux levels.

The original code modeled the core with 6 axial planes and 25 radial nodes in each plane. That arrangement is shown in Figure 1. Transient runs were made with the nodalization decreased to 54 nodes (9 radial by 6 axial - Figure 2), and increased to 294 nodes (49 radial by 6 axial - Figure 3), 588 nodes (98 radial by 6 axial - Figure 4), and 1014 nodes (169 radial by 6 axial - Figure 5),

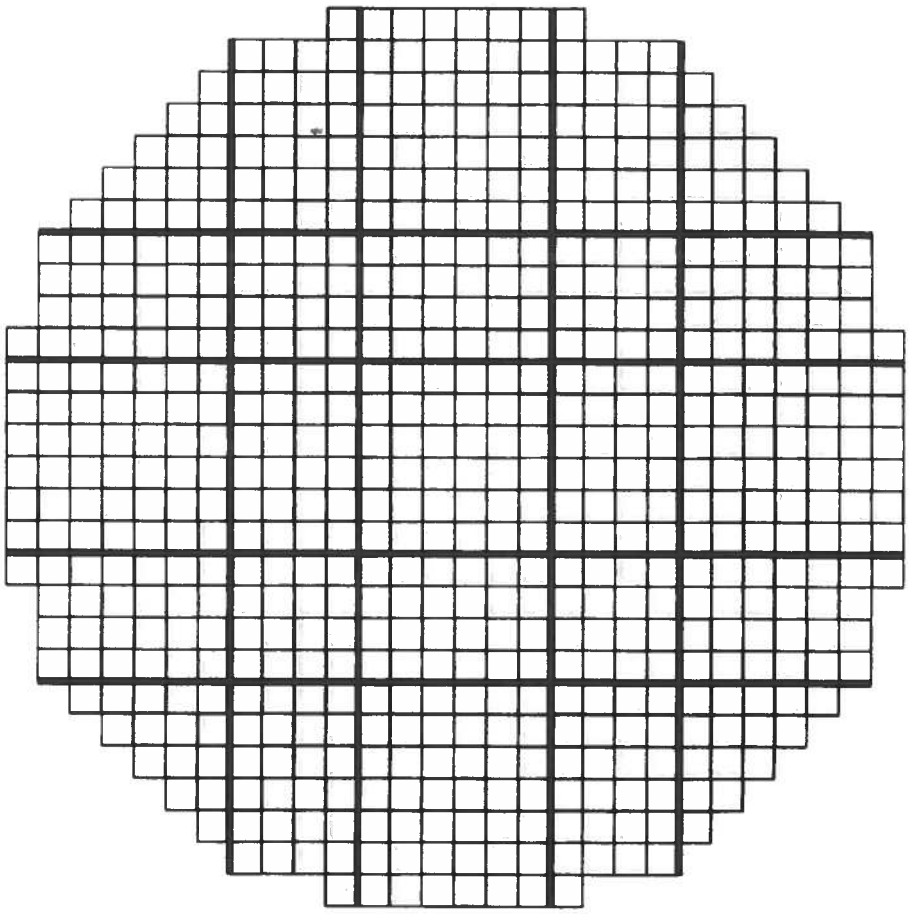

Figure 1 - 25 x 6 Node Core Diagram

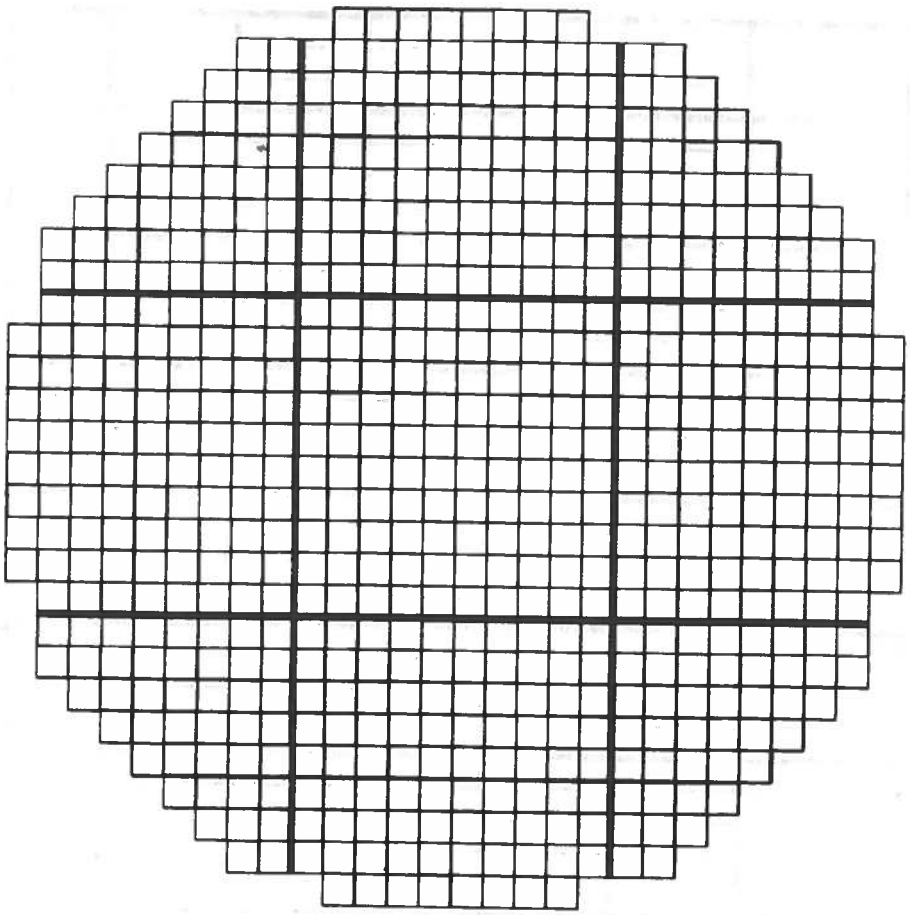

Figure 2 - 9 x 6 Node Core Diagram

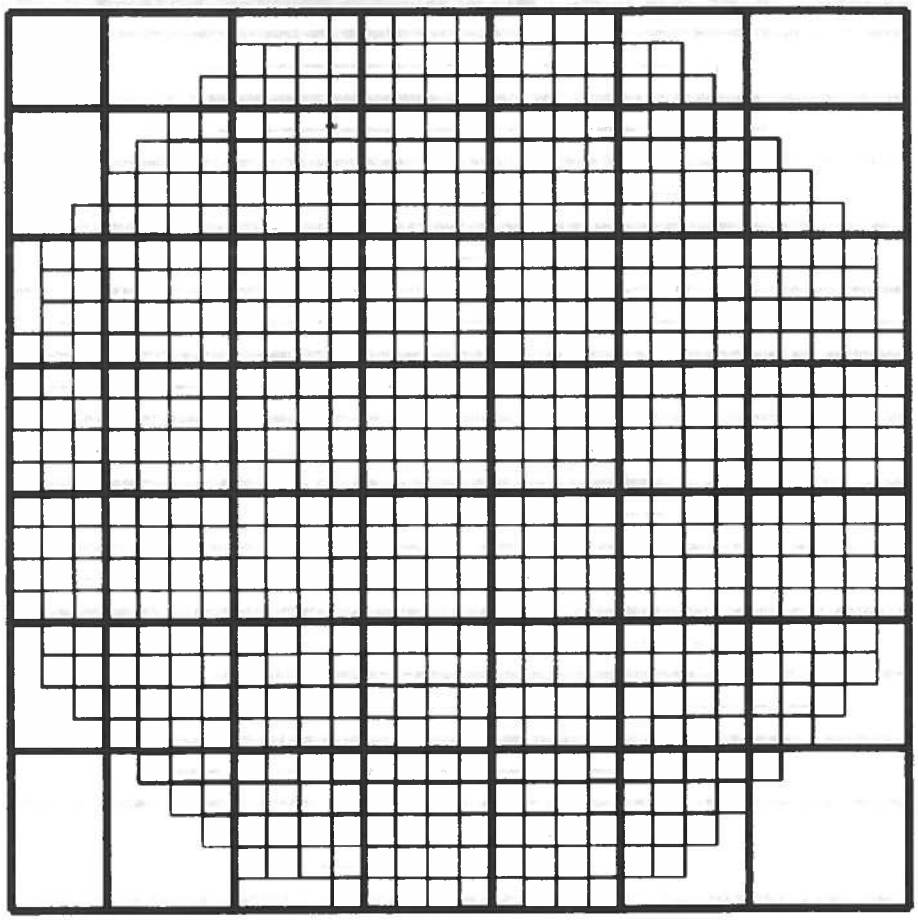

Figure 3 - 49 x 6 Node Core Diagram

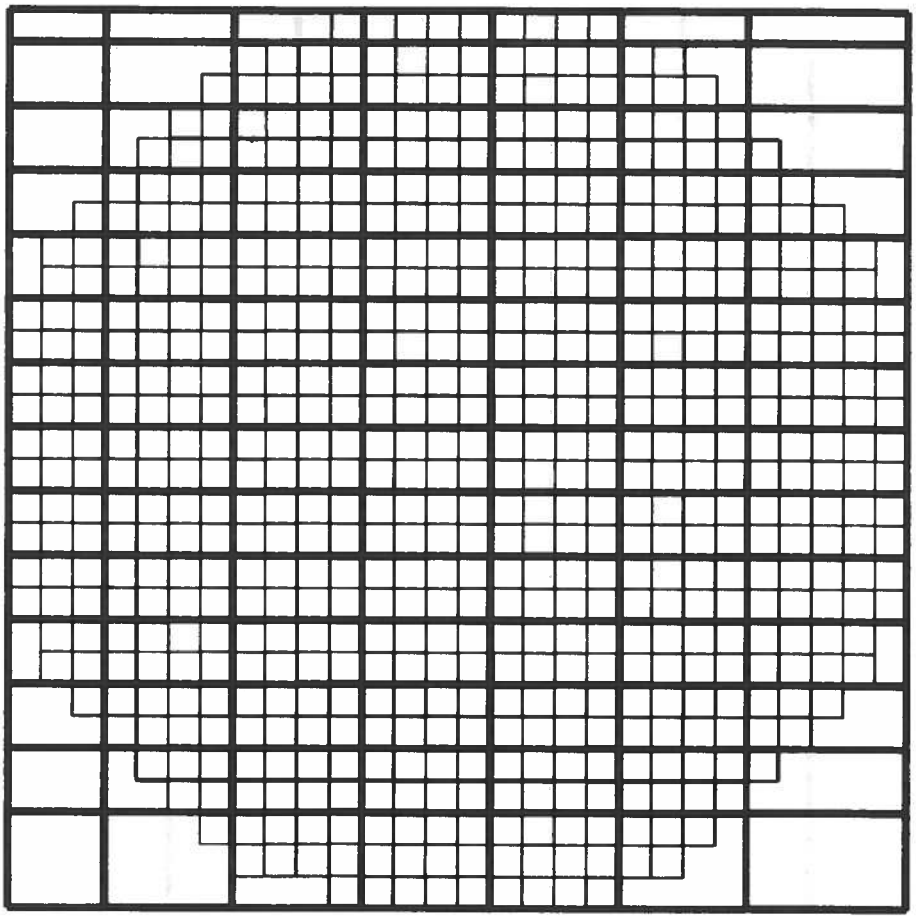

Figure 4 - 98 x 6 Node Core Diagram

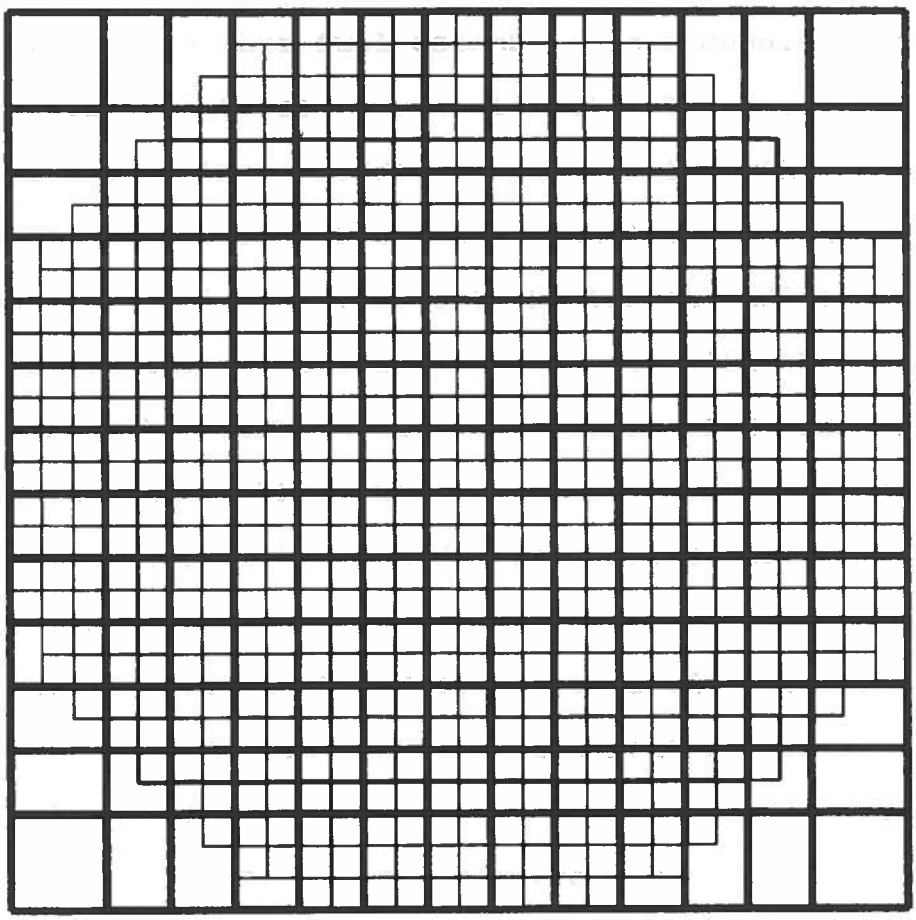

Figure 5 - 169 x 6 Node Core Diagram

respectively. The FLARE code was originally written for the Big Rock Point reactor where the control rods were inserted within the boundary of a fuel cell. Modern BWR's locate cruciform shaped control rods between four fuel assemblies. The four fuel assemblies surrounding a control rod are referred to as a control cell. The River Bend core contains 145 of these rodded control cells. The unrodded peripheral fuel assemblies can be modeled with an additional 24 cells. That set the finest radial nodalization that is easily accommodated with this code to 169 nodes. This particular code requires a square array at each axial plane. The 49x6, 98x6, and 169x6 nodalizations required empty peripheral nodes in order to satisfy this code requirement.

A sample transient had to be selected to compare performance of the model at the different levels of nodalization. The transient needed to produce a localized core effect. The transient selected was a control rod drop accident. This transient provides the advantage that localized effects can be initiated in different locations within the core.

A control rod drop accident is a design basis accident for boiling water reactors. In a BWR the control rods are hydraulically inserted from below the reactor vessel. The presumption for initiating the accident is that the control rod actuator is withdrawn to a position below the core, but

that the control rod is not mechanically coupled to the actuator and for some reason sticks in the fully inserted position. At some later time, the stuck control rod becomes released and free-falls until it makes contact with the actuator. The position instrumentation system for the control rods actually indicates the actuator position. This means that the reactor operator has no direct indication of the dropping control rod. The indication that a transient has occurred is limited to reactor power level instrumentation.

The reactor power level instrumentation consists of 132 fission chambers located in the channels between fuel assemblies. The fission chambers are arranged in 33 strings of 4 chambers axially positioned respectively, at 19, 55, 91, and 127 inches above the bottom of the core. The active core height is 144 inches. The radial positions of these fission chambers, referred to as Local Power Range Monitors (LPRMs), are indicated on Figure 6.

The reactor trip system receives input from the LPRMs as an indication of core power. Each of the 8 trip system channels takes input from either 16 or 17 LPRMs. The LPRMs associated with a particular trip system channel are helically selected so that each trip system channel receives input from multiple axial and radial areas of the core. Each LPRM provides an input to only one trip system channel and no channel receives input from more than one

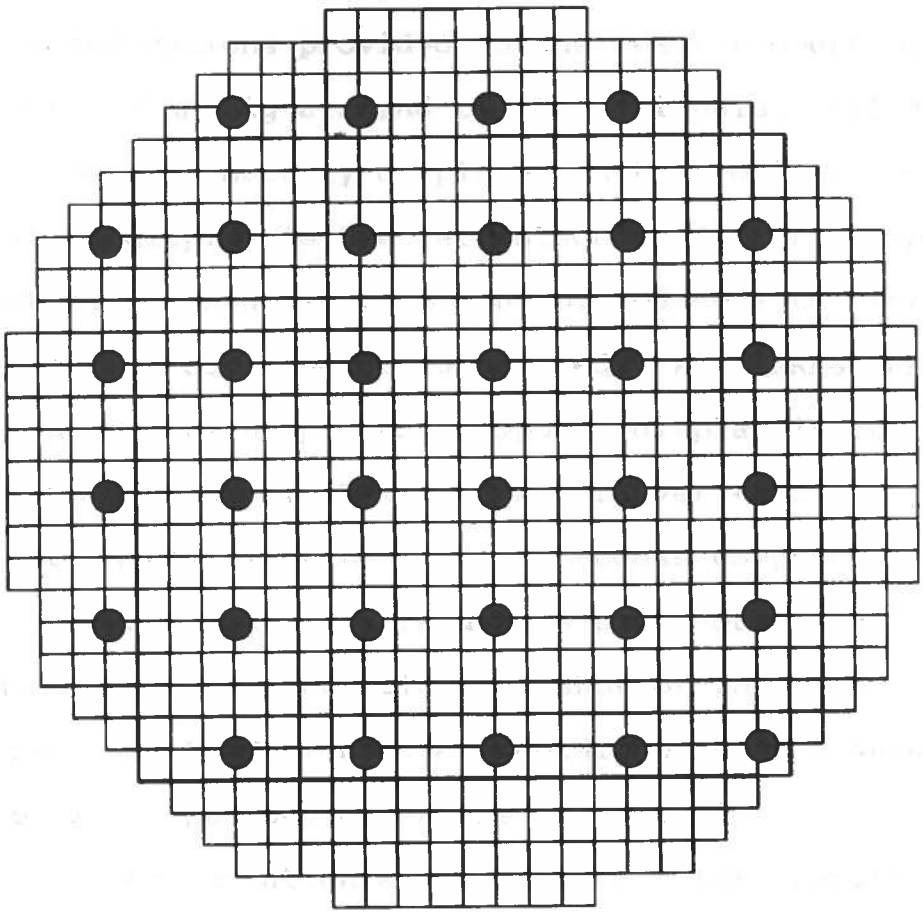

Figure 6 - Core LPRM Radial Loactions

LPRM in any one axial string. The trip system channels average the input from the LPRMs to create an Average Power Range Monitor (APRM) signal. There are eight APRMs. This arrangement is shown in Figure 7.

The indications provided to the reactor operator include the APRM signals and the LPRM signals. All 8 APRM signals are continuously displayed in the control room. The unit of display is the percentage of full rated power. The LPRM string nearest to a control rod selected for motion is also continuously displayed. All LPRMs can be displayed on a plant process computer display if desired by the reactor operator. This is one of over 40 displays available on the River Bend plant process computer. The reactor operator can also request a print out of all LPRM readings. This is a one time snapshot of the LPRM readings. The LPRM signals are conditioned to display in units of watts per cubic centimeter of fuel.

The instrumentation systems dictate the specific comparisons to be made at the various levels of core nodalization. The principle comparison is necessarily between APRM channel performance since this is the continuous indication to the operator and because this provides the trip system signal if the APRM level exceeds trip limits. The APRM trip limit is set at 117% of full rated reactor power. A secondary comparison is between the performance of the LPRMs.

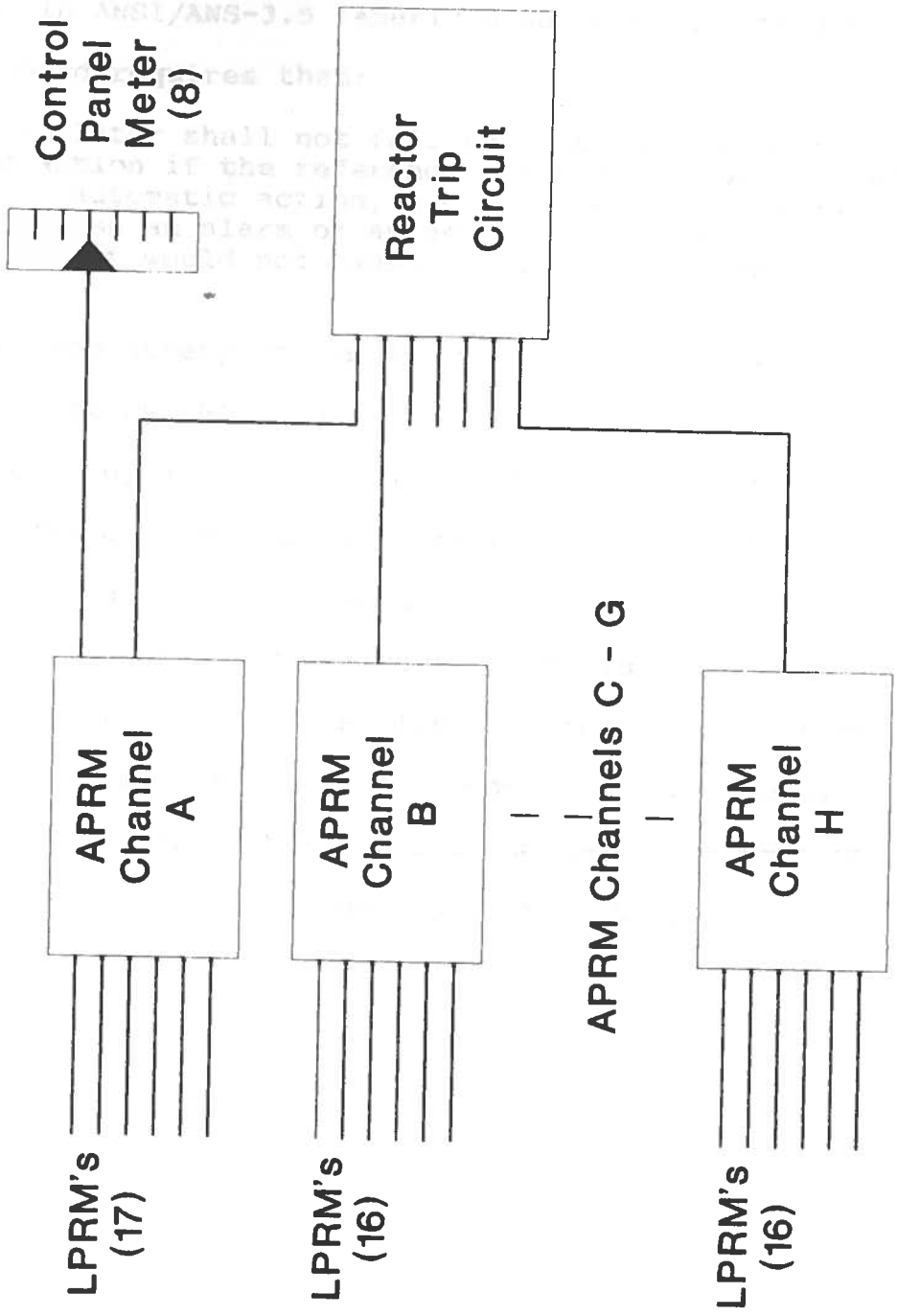

Figure 7 - Nuclear Instrumentation Block Diagram

The performance criteria for simulation models is described in ANSI/ANS-3.5 (American Nuclear Society 1985). This standard requires that:

"...the simulator shall not fail to cause an alarm or automatic action if the reference plant would have caused an alarm or automatic action, and conversely, the simulator shall not cause an alarm or automatic action if the reference plant would not cause an alarm or automatic action."

The River Bend safety analysis report (Gulf States Utilities Company 1987) describes the plant response to a control rod drop accident from full power at 50% rod density. The accident analysis predicts a reactor scram signal from high neutron flux within one second of the start of the event. The entire accident is terminated by the reactor trip in less than five seconds. Application of the requirements of ANS/ANSI-3.5 means that each model would have to predict at least two channels of APRM flux at greater than 117% to be judged as satisfactory.

CODE DESCRIPTION

The FLARE code is derived from a nodal version of the one group diffusion kinetics equation (Delp et al. 1964):

$$\Lambda \frac{d(S_{vn}V_n)}{dt} = (1-\beta)K_{\infty n}\left[\sum_m W_{mn}S_{vm}V_m + W_{nn}S_{vn}V_n\right] + \sum_{j=1}^{6}\lambda_j C_{vnj}V_n - S_{vn}V_n \quad (1)$$

$$\frac{d(C_{vnj}V_n)}{dt} = \beta_j K_{\infty n}\left[\sum_m W_{mn}S_{vm}V_m + W_{nn}S_{vn}V_n\right] - \lambda_j C_{vnj}V_n \ , j = 1,6 \quad (2)$$

where:

Λ = neutron lifetime (sec)

S_{vn} = neutrons produced in node n (n/cm^3-sec)

V_n = volume of node n (cm^3)

β = delayed neutron fraction

$K_{\infty n}$ = infinite multiplication factor in node n

W_{mn} = probability that a neutron born in node m will be absorbed in node n

W_{nn} = probability that a neutron born in node n will be absorbed in node n

λ_j = decay constant for precursor group j (sec^{-1})

C_{vnj} = concentration of precursor group j in node n ($atoms/cm^3$)

β_j = delayed neutron fraction of precursor group j

In the above equations, K_{en}, W_{mn}, and the unknowns S_{vn} and C_{vnj} are functions of space and time. The common assumption can be made that the neutron production rate can be factored into a shape function $\Psi_{vn}(r,t)$ and an amplitude function T(t) (Henry 1986). A further assumption is made that the shape function is slowly varying compared with the amplitude function such that $\Psi_{vn}(r,t) = \Psi_{vn}(r)$.

The quasi-static nodal shape function can then be written as:

$$S_n = \frac{V_n S_{vn}}{\sum_n V_n \psi_{vn}} = \psi_n T \qquad (3)$$

$$\psi_n = \frac{V_n \psi_{vn}}{\sum_n V_n \psi_{vn}} \qquad (4)$$

where:

S_n = neutrons produced in node n (n/sec)

Ψ_n = relative shape in node n

Summing the nodal neutron production rate across all nodes gives:

$$\sum_n S_n = (\sum_n \psi_n) T \qquad (5)$$

At the critical condition, the total shape function is normalized such that:

$$\sum_n \psi_n = 1 \qquad (6)$$

Dividing Equations 1 and 2 by $\Sigma v_n \Psi_{vn}$ yields:

$$\Lambda \frac{dS_n}{dt} = (1-\beta) K_{\infty n} [\sum_m W_{mn} S_m + W_{nn} S_n] + \sum_j \lambda_j C_{nj} - S_n \qquad (7)$$

$$\frac{dC_{nj}}{dt} = \beta_j K_{\infty n} [\sum_m W_{mn} S_m + W_{nn} S_n] - \lambda_j C_{nj} \qquad (8)$$

where:

$$C_{nj} = \frac{V_n C_{vnj}}{\sum_n V_n \psi_{vn}}$$

Solution of the shape function uses the assumption that the shape function varies slowly and that the time variation of the precursors with respect to the shape function is very slow. Equations 7 and 8 can be set equal to zero. Solution of Equations 7 and 8 for the shape function yields:

$$\psi_n = \frac{K_{\infty n}}{\lambda} [\sum_m W_{mn} \psi_m + W_{nn} \psi_n] \qquad (9)$$

where:

λ = an eigenvalue of the solution matrix

Solution of Equations 7 and 8 for the amplitude function yields a simple point kinetics solution:

$$\frac{dT}{dt} = \frac{(\rho-\beta)}{\Lambda} T + \sum_j \lambda_j C_j \qquad (10)$$

$$\frac{dC_j}{dt} = \frac{\beta_j}{\Lambda} T - \lambda_j C_j \qquad (11)$$

The nodal reactivity (ρ) accounts for xenon, samarium, boron, fuel temperature, moderator temperature, and fission cross section effects. Two fuel analysis programs, Casmo and Simulate, are used to obtain fuel bundle cross section data. The nodal nuclear properties for each parameter are collapsed from Casmo and Simulate 24 x 624 mesh data through determination of nodal B-constants (Lynn Leatherwood, letter to the author, March 1994). The general method utilized to account for the reactivity effect of some parameter P is:

$$\left(\frac{\Delta K}{K}\right)_P(ARO) = B_1 + B_2\rho + B_3\rho^2 \qquad (12)$$

$$(\frac{\Delta K}{K})_P(ARI) = B_4 + B_5\rho + B_6\rho^2 \qquad (13)$$

$$(\frac{\Delta K}{K})_P = (\frac{\Delta K}{K})_P(ARI) + [(\frac{\Delta K}{K})_P(ARO) - (\frac{\Delta K}{K})_P(ARI)]f \qquad (14)$$

Equations 12 and 13 determine reactivity of parameter P for the rodded (ARI) and unrodded condition (ARO) based on a second order curve fit to nodal liquid density. Equation 14 is used to find the net reactivity effect of parameter P for the actual nodal rodded fraction (f).

The nodal coupling coefficients (W_{mn} and W_{nn}) are determined from the lattice-physics data, collapsing the nodal two group data into a single migration area for each node. The migration area is determined for a rodded and unrodded configuration so that it can be linearly varied based on the fraction of control rod insertion within the node. The migration areas employ a nodal curve fit based on mixture moderator density. The nodal infinite multiplication factor ($K_{\infty n}$) is corrected with curve fits of the nodal physics data for the effects of fuel burnup, doppler, boron, xenon, and samarium. Constant albedos are tuned to account for reflector effects on the peripheral and end nodes.

The use of the FLARE code requires a number of implicit assumptions. First as with any space-time kinetics model it is assumed that nodal kinetics can be

modeled by a set of slowly varying conditions. This is an acceptable assumption provided that the positive core net reactivity is much less than the delayed neutron fraction (Beta) such that the rate of power is limited to a reasonable value.

Second, FLARE assumes that an albedo boundary condition is adequate. This would be a poor assumption for a small compact core geometry but for large commercial reactors where the external leakage is a small fraction of the internal flux this is another acceptable assumption.

Third, an assumption must be made that a neutron born in one node will be absorbed in either that node or in one of the six neighboring nodes. This assumption is necessary because FLARE does not take into account any neutron migration beyond those six adjacent nodes. This assumption is acceptable provided that the node dimensions are large compared to the neutron diffusion length. The finest nodalization for this project provided node dimensions at least 1.5 times that of the original Big Rock Point FLARE node dimensions.

The control rod drop transient flux peak is limited by the Doppler feedback from the fuel temperature effect. To provide this feedback, a limited thermodynamic model was required. The required extent of this model was limited by the duration of the transient of interest. In the few seconds of interest, an assumption can be made that no

change in the fluid channel conditions would occur as long as a margin to a critical heat flux is maintained. This means that the additional power produced would all be retained in the fuel rods and contribute completely to the fuel temperature rise. A lumped parameter approach was used to model heat transfer through the fuel rods.

A heat balance can be described across the fuel pellet for a solid cylindrical pellet (Kazimi and Todreas 1989):

$$T_m - T_{fo} = \frac{q'}{8\pi k} \qquad (15)$$

where:

T_m = average fuel temperature (K)

T_{fo} = pellet outer temperature (K)

q' = linear heat rate (W/m)

k = pellet thermal conductivity (W/m-K)

A heat balance across the fuel gap can be described:

$$T_{fo} = T_{ci} + \frac{q'}{2\pi R_g h_g} \qquad (16)$$

where:

T_{ci} = clad inner wall temperature (K)

R_g = mean gap radius (m)

h_g = gap conductance (W/m^2-K)

Solving Equations 15 and 16 to eliminate pellet outer temperature:

$$T_m = T_{ci} + \frac{q'}{2\pi R_g h_g} + \frac{q'}{8\pi k} \qquad (17)$$

With the clad inner wall temperature fixed at some initial value, the fuel mean temperature can be determined from the fuel linear heat generation rate.

The code solution for the neutronics equations was performed at four iterations per second. The thermodynamic solution was performed at sixteen cycles per second. These frequencies were determined by the vendor of the code. A block diagram of the solution sequence and frequencies is provided in Figure 8.

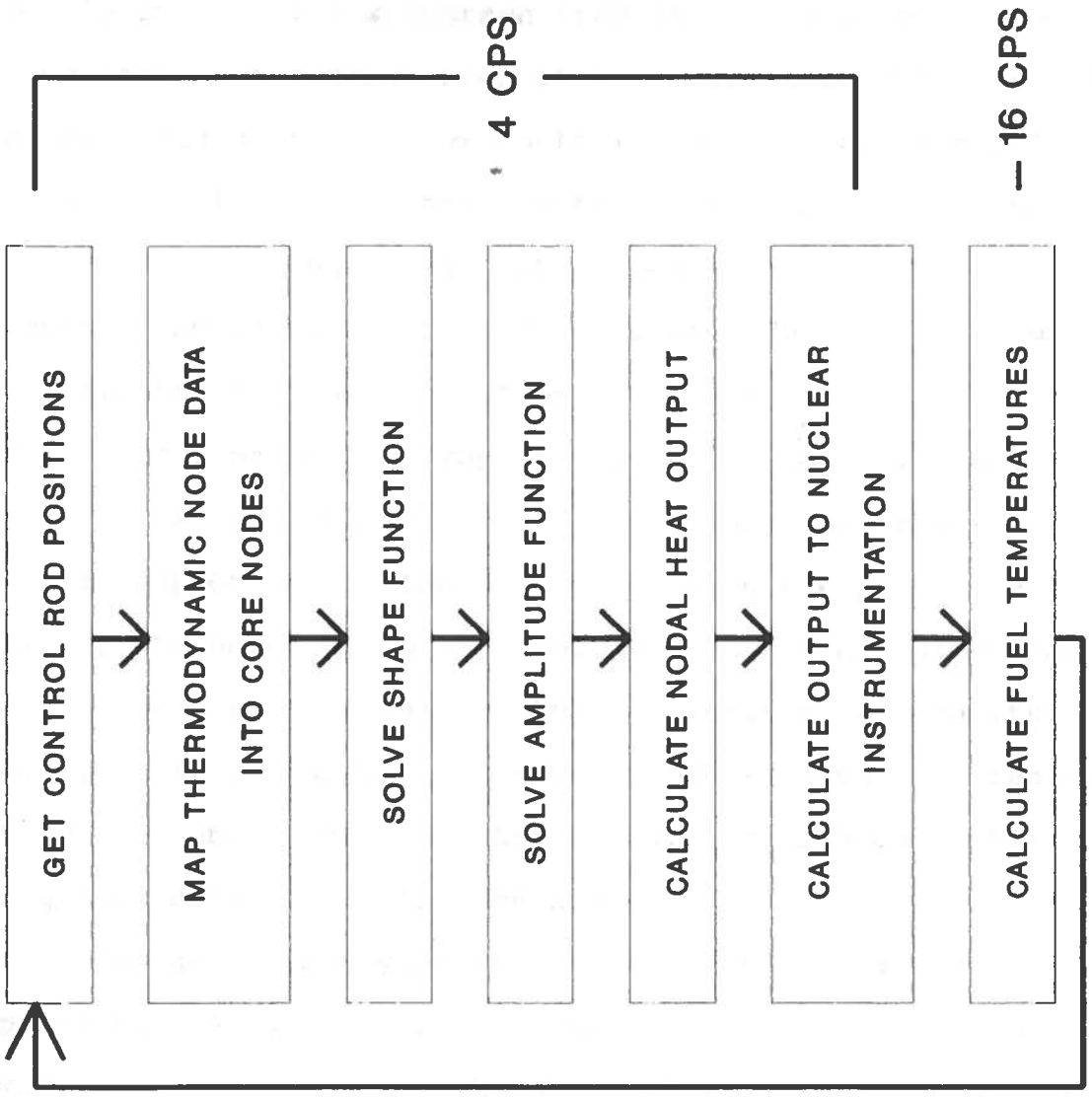

Figure 8 - Code Block Diagram

RESULTS

The River Bend cycle four middle of cycle 100% power conditions predicted 136 of the 145 control rods either partially or fully withdrawn from the reactor core. The nine remaining control rods at this target condition would be arranged as the center control rod and eight control rods in a ring around that center control rod being fully inserted. The model was initialized with this target control rod pattern for each level of nodalization. Two transients were initiated from equilibrium conditions. The first transient was a drop of the center control rod (designated as control rod 28-29). The second transient was a drop of one of the control rods in the peripheral ring (designated as control rod 20-21). Each control rod was allowed to free fall at the acceleration of gravity until fully withdrawn. Data was taken at each 0.25 second time step until the flux stabilized. In each case, this required a total of six time steps.

The safety analysis for the River Bend reactor predicts that a reactor trip condition would be sensed within one second after the start of the control rod drop accident and the flux peak will be terminated by the control rod scram insertion within five seconds after the start of the accident (Gulf States Utilities Company 1987). To ensure that the entire transient peak would be captured,

all LPRM data was captured at one-fourth second intervals for the first six time steps of the transient at each level of nodalization. The LPRM data was then normalized to the time = 0 value to provide an indication of the variation of each LPRM during the transient. This data is presented in Figures 9 through 18.

The control rod position at the first time step (t=1) is 12 inches withdrawn. At the second time step (t=2) the control rod is 48 inches withdrawn. At the third time step (t=3) the control rod is 108 inches withdrawn. The control rod is fully withdrawn at the fourth through sixth time steps. LPRM string D (channels 100-132) is located at the 23 inch withdrawn position. LPRM string C (channels 67-99) is at location 59 inches, string B (channels 34-66) at 95 inches, and string A (channels 1-33) at 131 inches.

Control rod 28-29 is immediately adjacent to the LPRM string labeled channel 20, 53, 86, and 119. Control rod 28-29 is surrounded by LPRMs 13-15, 19-21, 25-27 at the lowest elevation, 46-48, 52-54, 58-60 at the next elevation, 79-81, 85-87, 91-93 at the third elevation, and 112-114, 118-120, 124-126 at the upper elevation. Control rod 20-21 is immediately adjacent to LPRMs 13, 46, 79, and 112 and is surrounded by a similar set of neighboring LPRMs. The LPRM data for each level of nodalization indicate the control rod tip near the upper string of LPRMs

at the first time step and continuing to move down to being fully withdrawn by the fourth time step. The width of the LPRM flux peak indicates the volume of the core that the nodalization spreads the power spike.

The reactor trip is initiated when the APRM levels on multiple channels exceeds 117%. The APRM flux levels for the control rod 28-29 and control rod 20-21 drop events are provided in Tables 1 and 2.

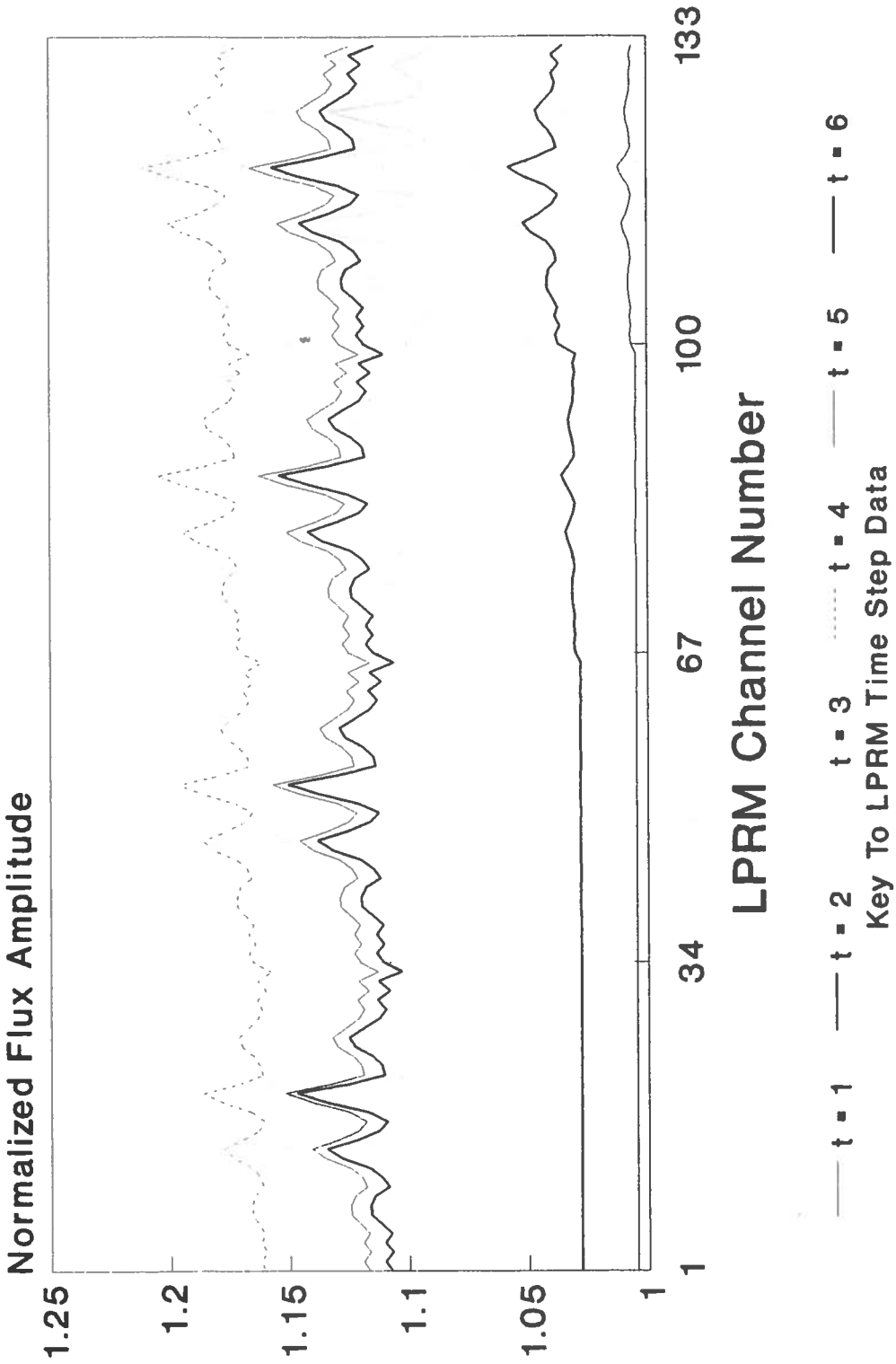

Figure 9 - 9 x 6 Array Rod Drop Data Rod 28-29

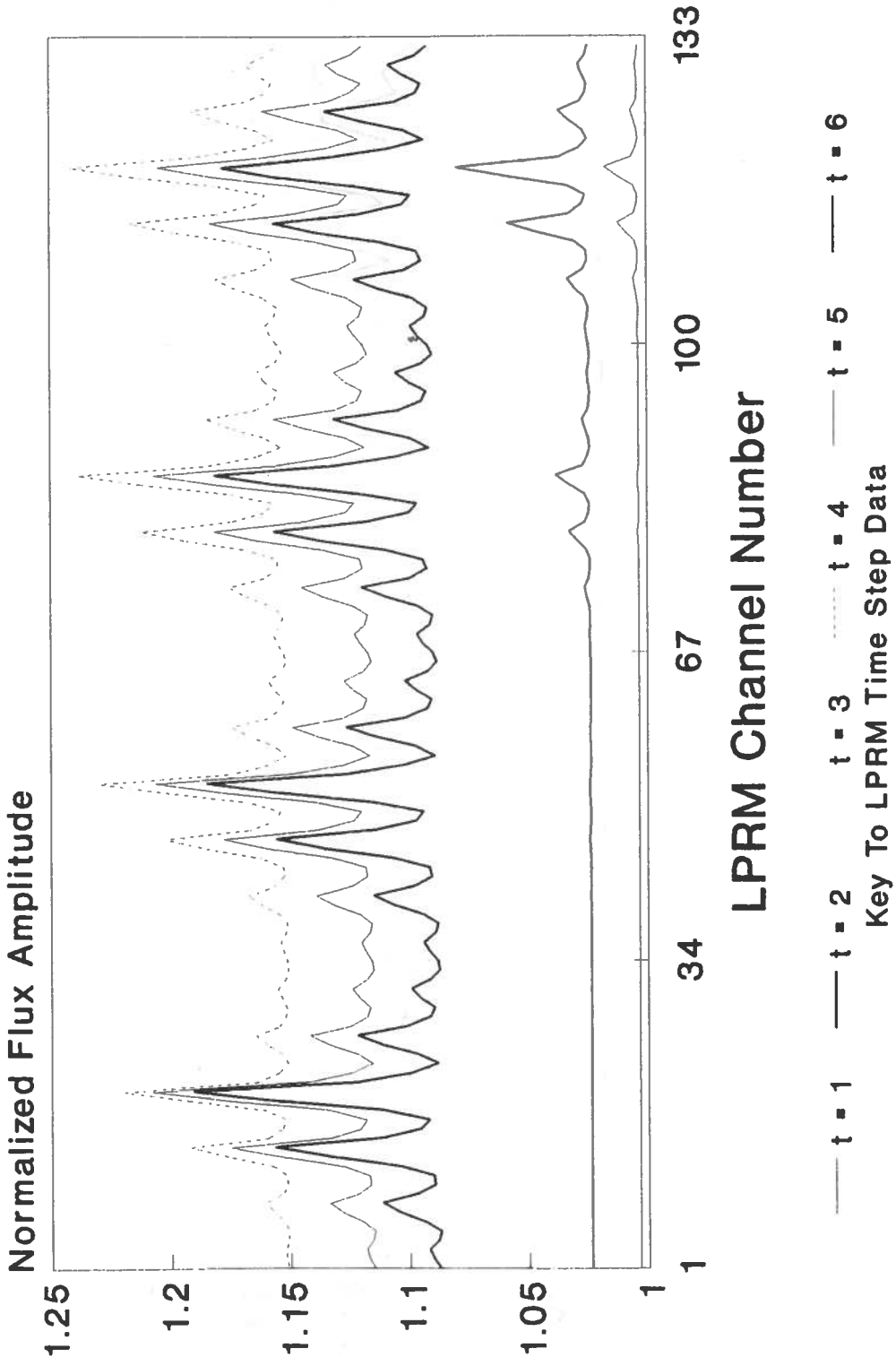

Figure 10 - 25 x 6 Array Rod Drop Data Rod 28-29

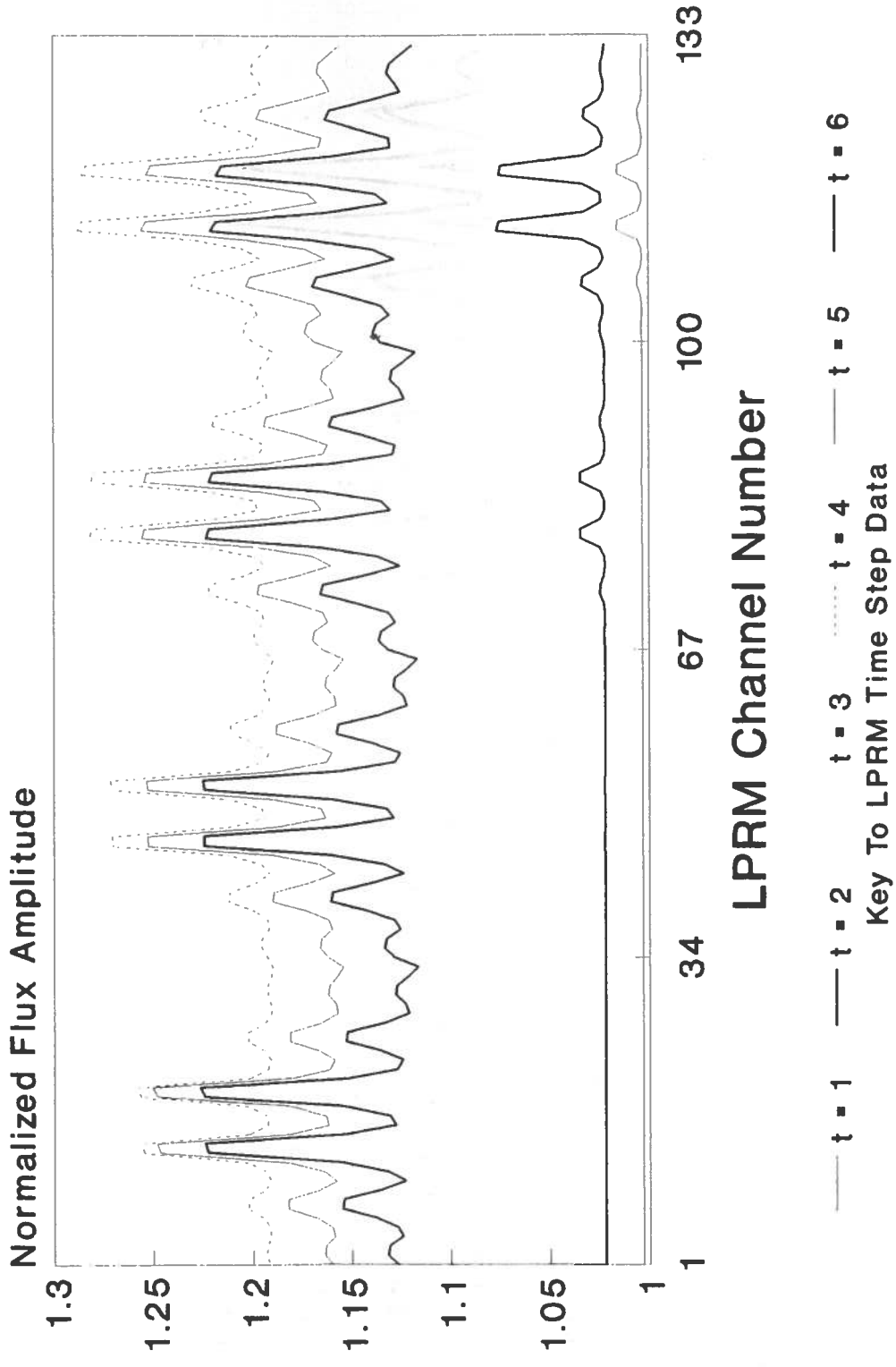

Figure 11 - 49 x 6 Array Rod Drop Data Rod 28-29

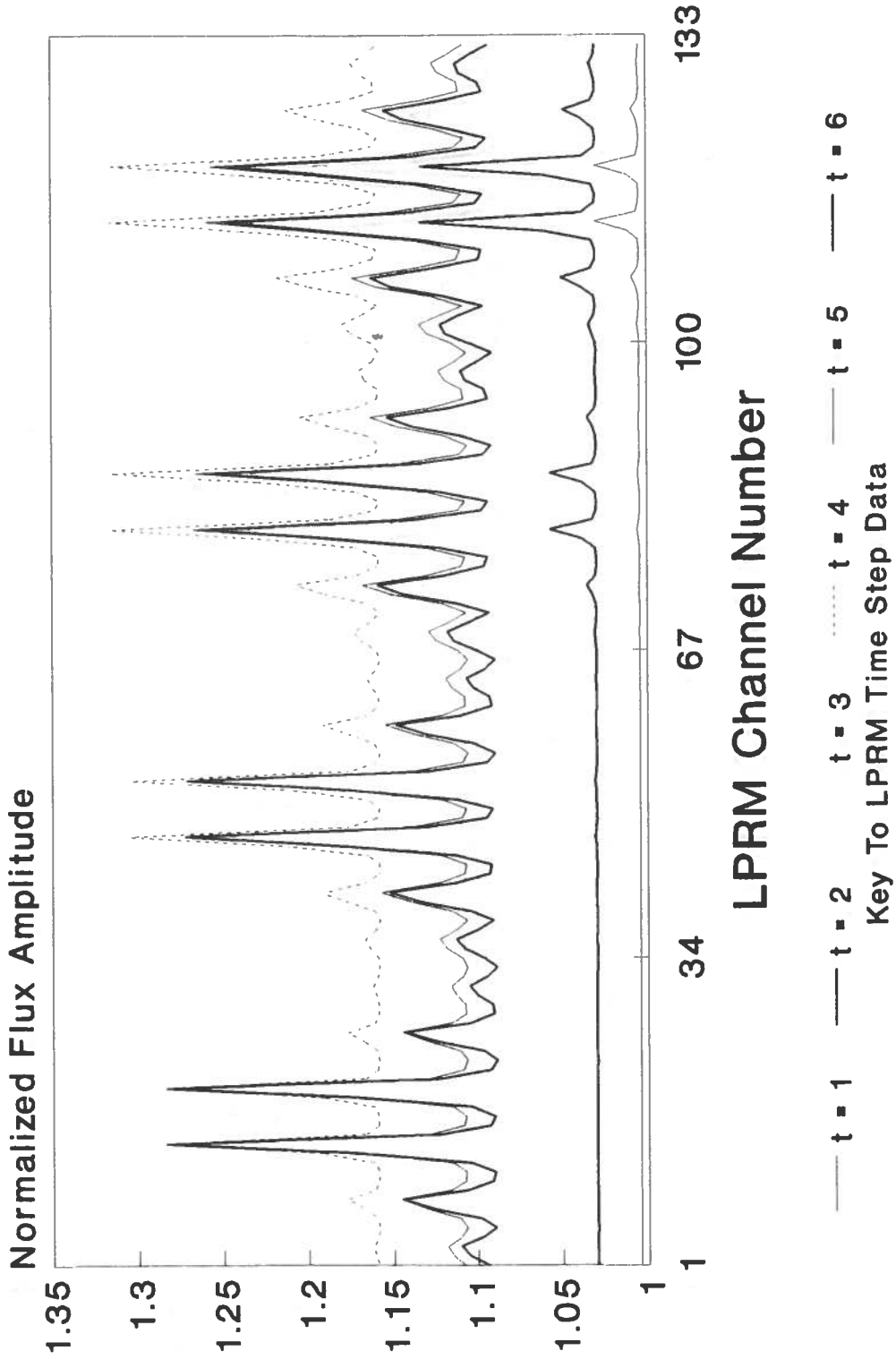

Figure 12 - 98 x 6 Array Rod Drop Data Rod 28-29

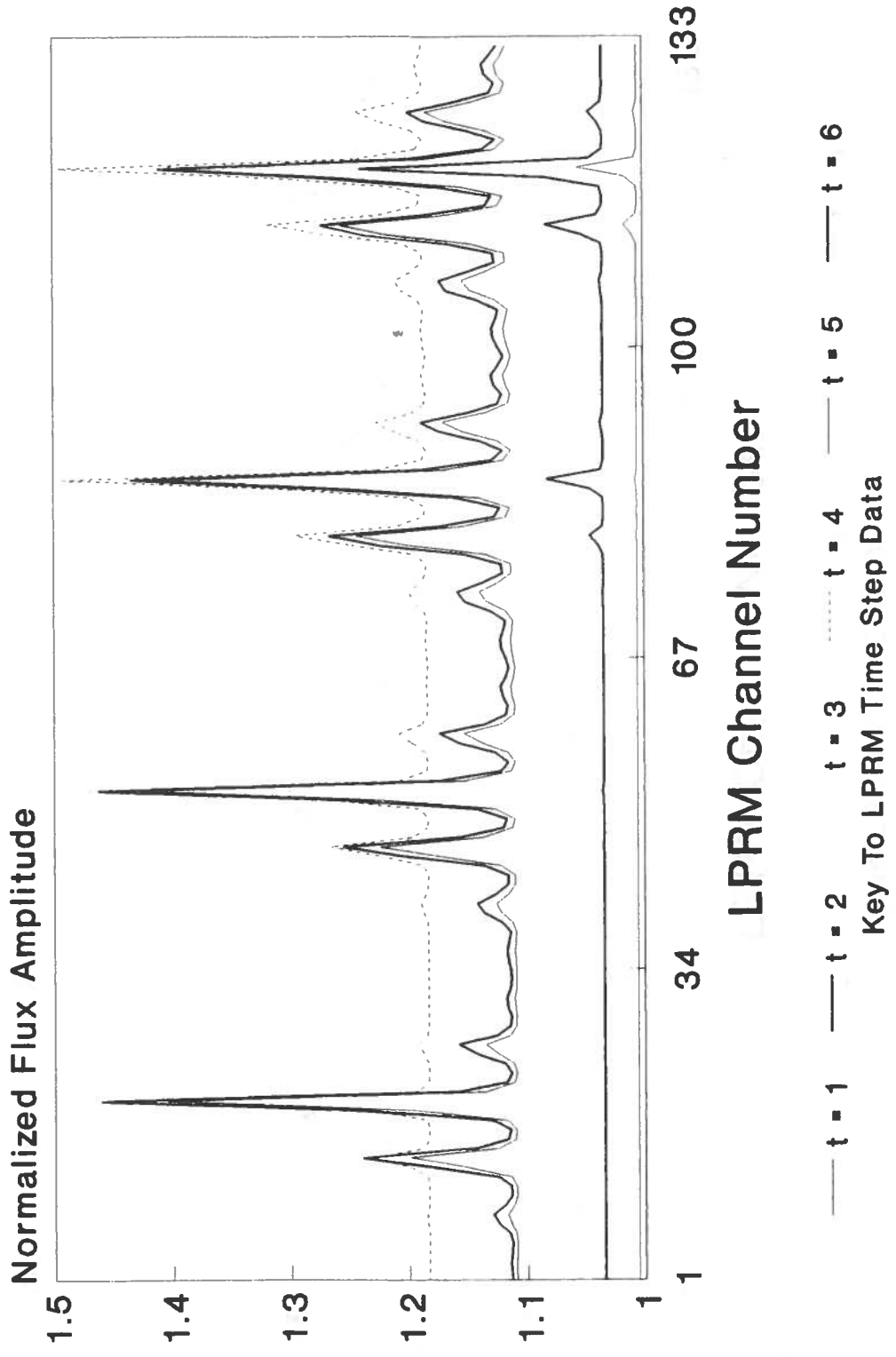

Figure 13 - 169 x 6 Array Rod Drop Data Rod 28-29

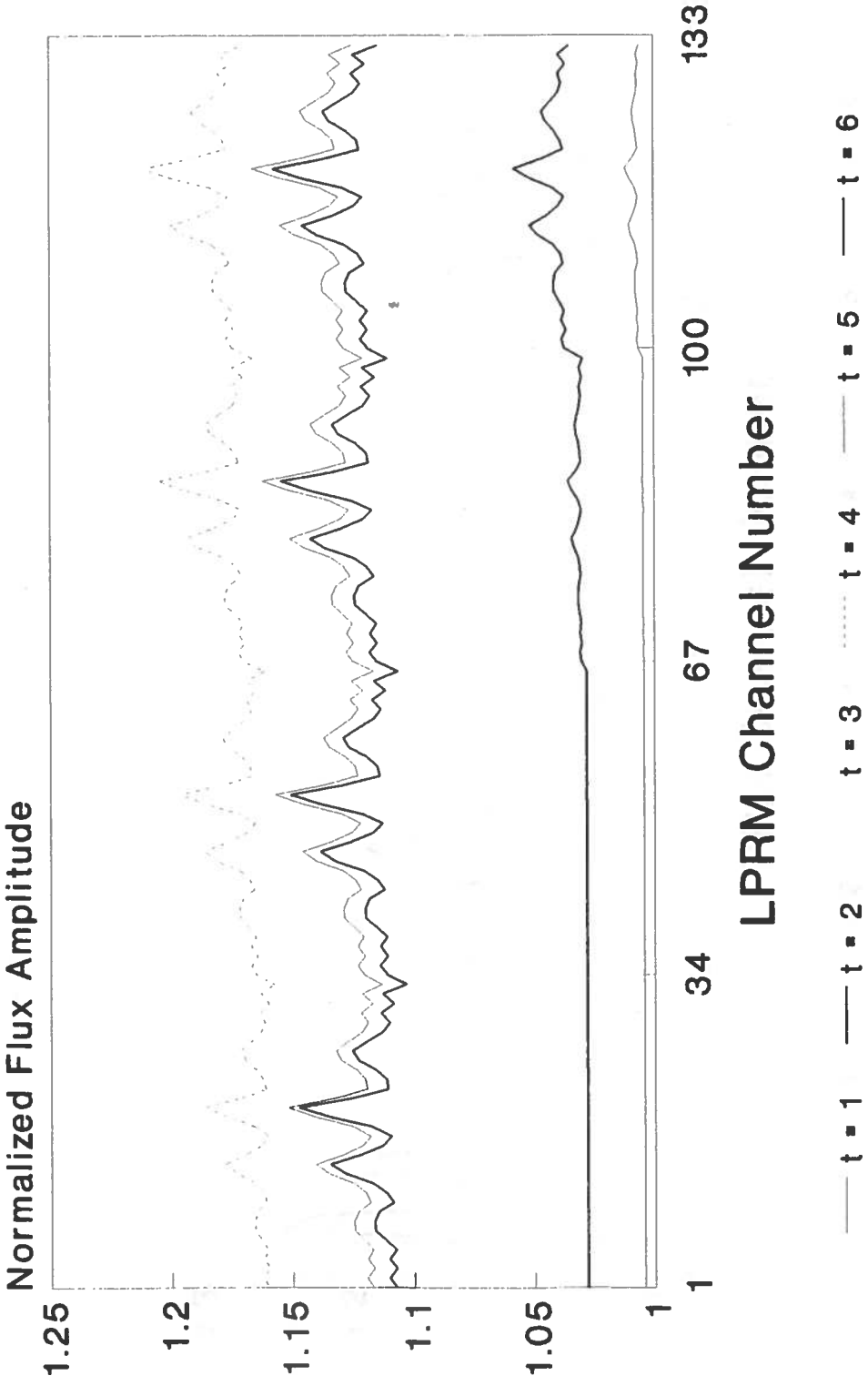

Figure 14 - 9 x 6 Array Rod Drop Data Rod 20-21

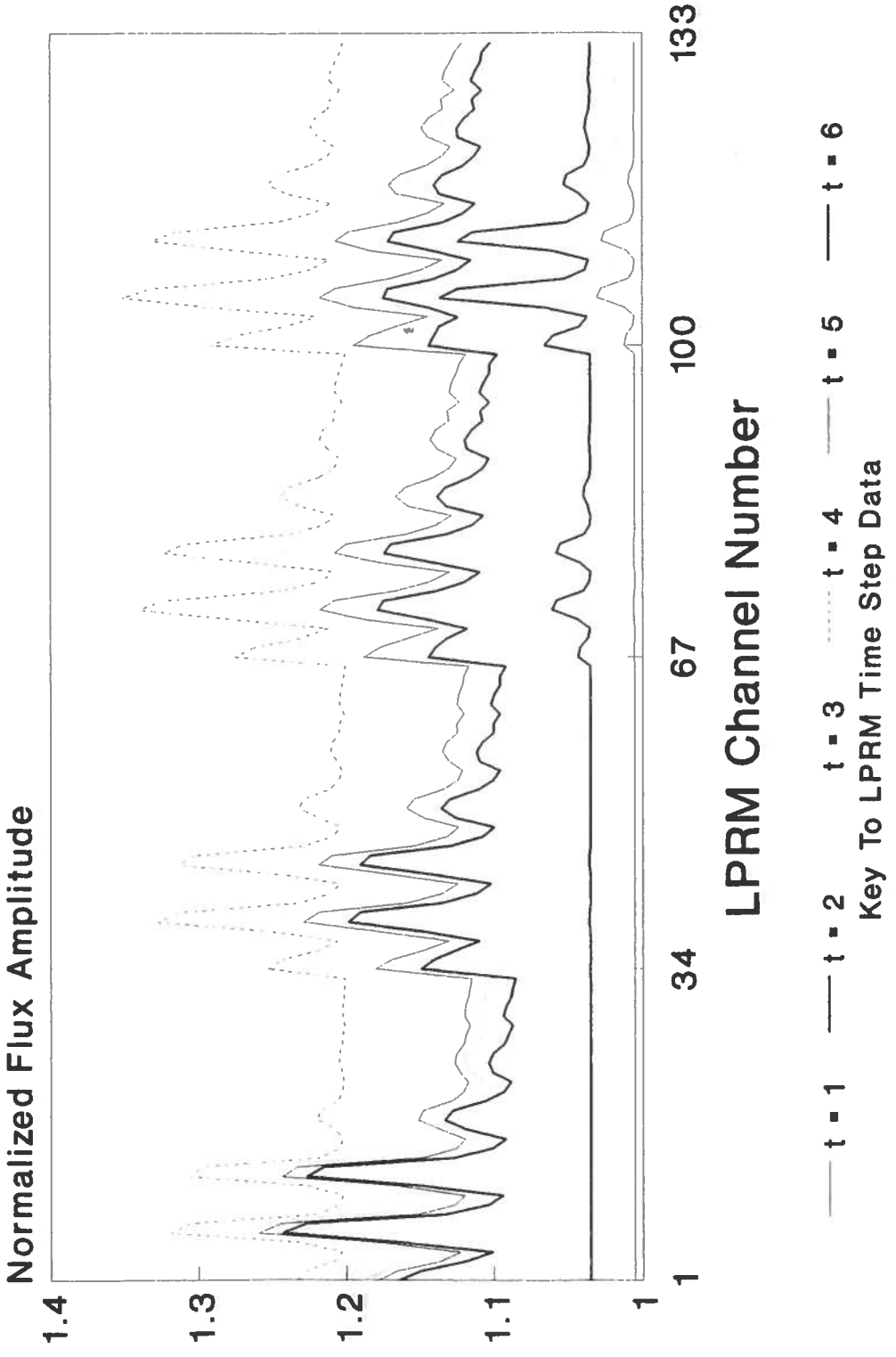

Figure 15 - 25 x 6 Array Rod Drop Data Rod 20-21

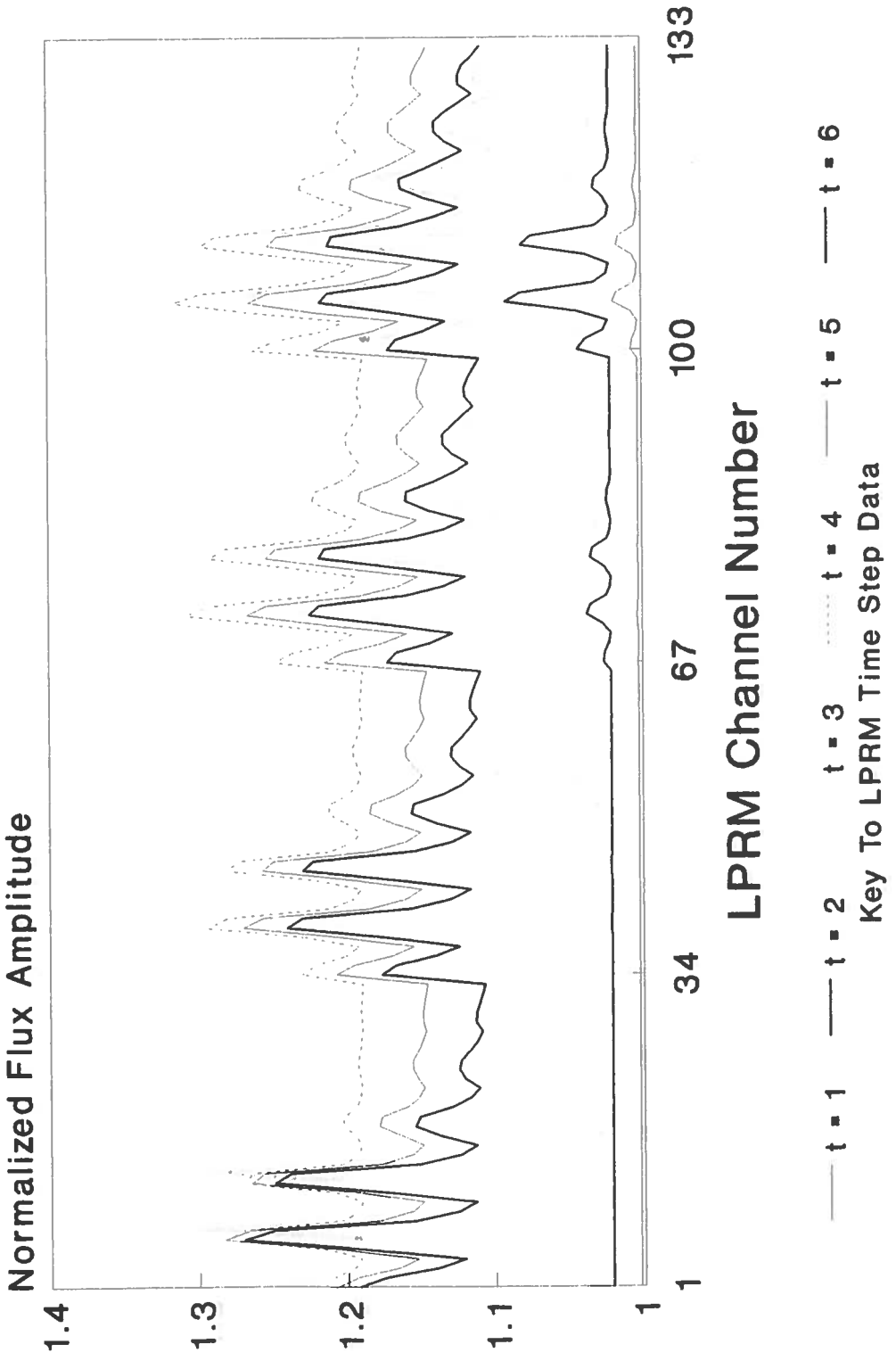

Figure 16 - 49 x 6 Array Rod Drop Data Rod 20-21

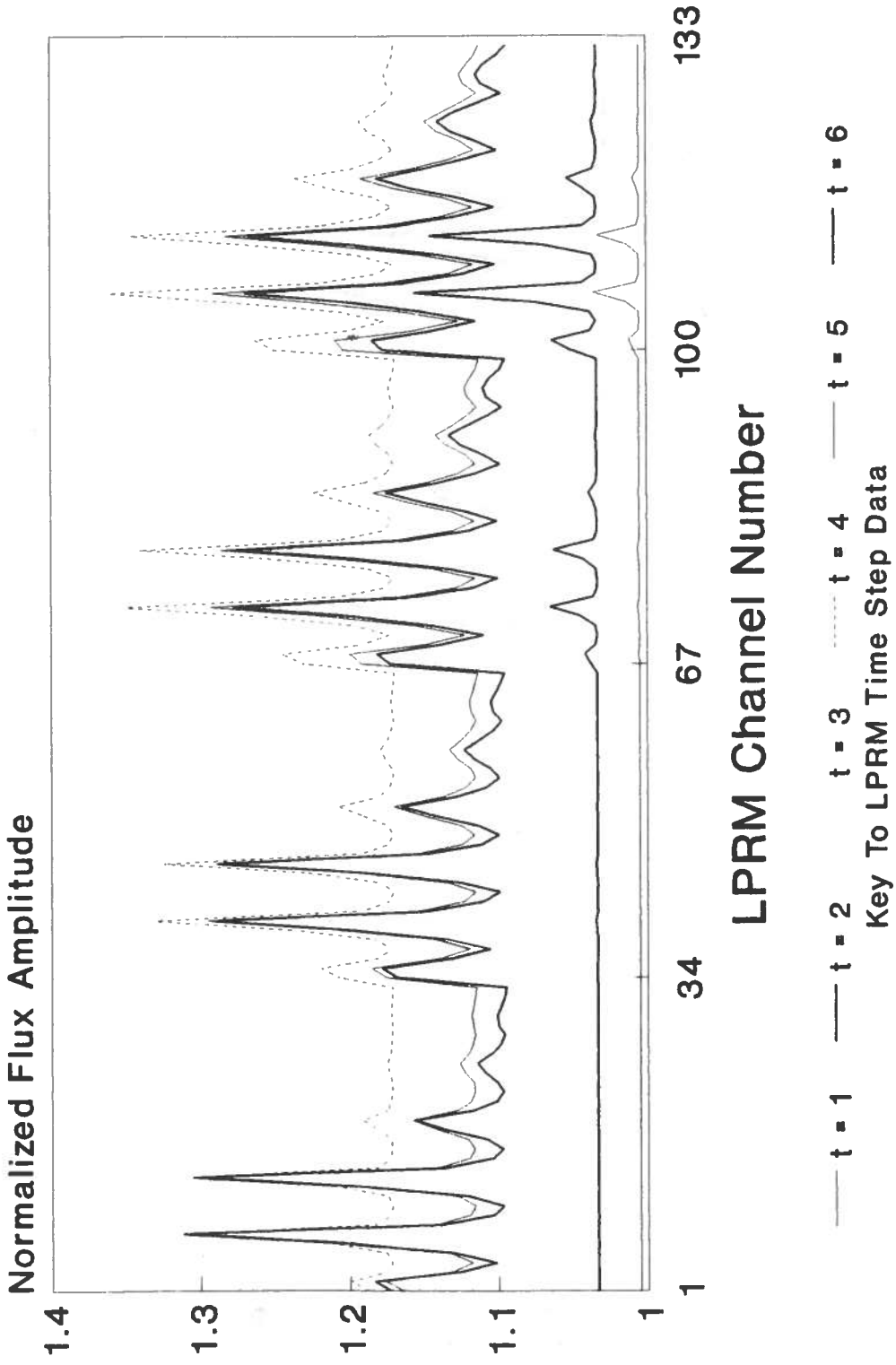

Figure 17 - 98 x 6 Array Rod Drop Data Rod 20-21

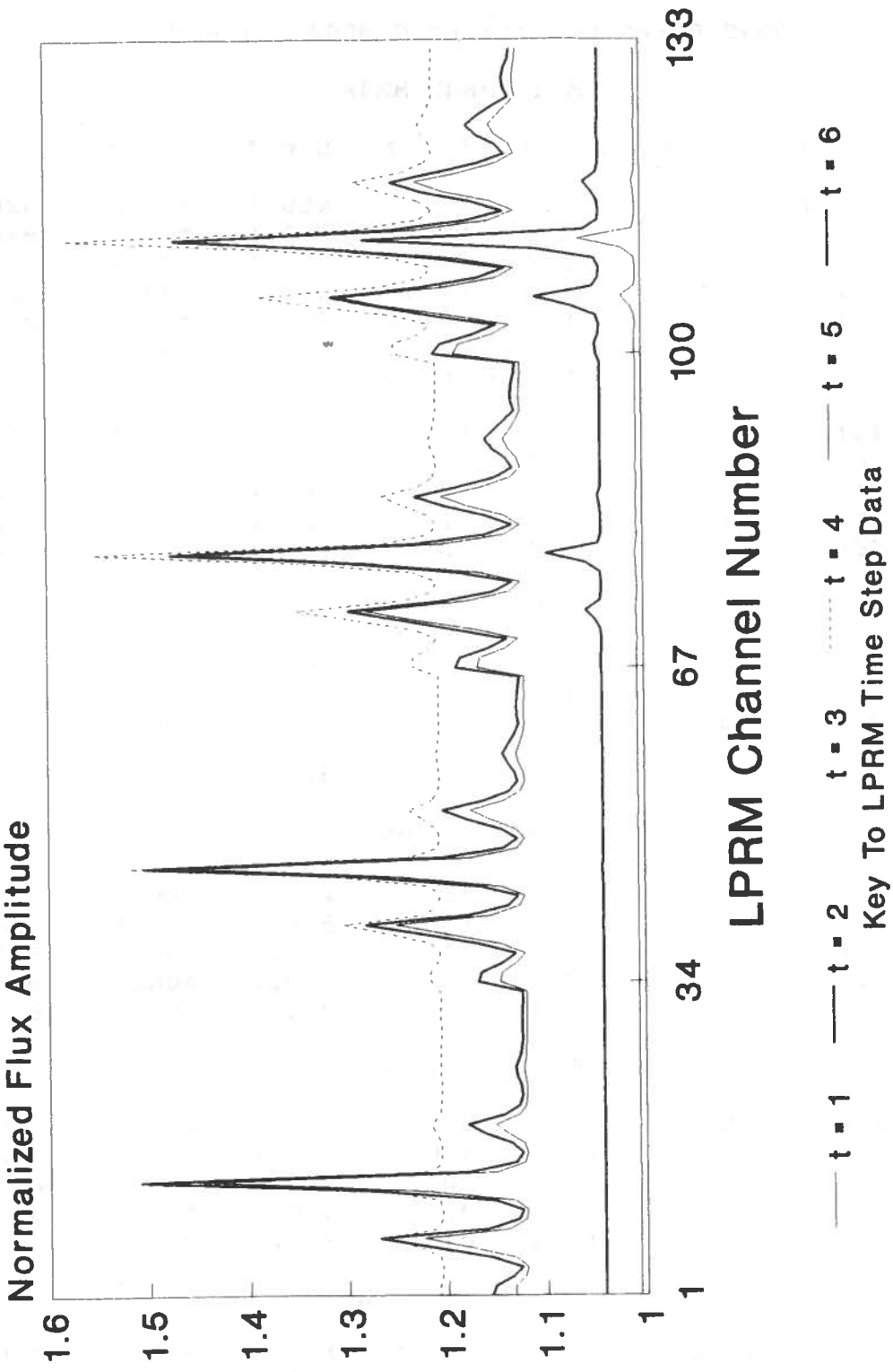

Figure 18 - 169 x 6 Array Rod Drop Data Rod 20-21

Table 1 - APRM Data for Rod 28-29 Drop

APRM Channel A

Nodes	t = 1	t = 2	t = 3	t = 4	t = 5	t = 6
9x6	1.005	1.032	1.114	1.175	1.132	1.123
25x6	1.004	1.025	1.099	1.166	1.135	1.109
49x6	1.003	1.024	1.113	1.212	1.183	1.150
98x6	1.005	1.032	1.119	1.183	1.138	1.128
169x6	1.005	1.035	1.137	1.210	1.147	1.161

APRM Channel B

9x6	1.006	1.033	1.115	1.174	1.130	1.121
25x6	1.004	1.026	1.100	1.165	1.132	1.106
49x6	1.004	1.026	1.113	1.210	1.181	1.147
98x6	1.005	1.033	1.119	1.179	1.132	1.120
169x6	1.005	1.036	1.145	1.211	1.145	1.157

APRM Channel C

9x6	1.006	1.033	1.114	1.174	1.131	1.122
25x6	1.004	1.028	1.101	1.167	1.136	1.111
49x6	1.004	1.026	1.113	1.211	1.183	1.150
98x6	1.006	1.037	1.120	1.180	1.136	1.126
169x6	1.006	1.038	1.140	1.204	1.138	1.151

APRM Channel D

9x6	1.004	1.029	1.112	1.172	1.129	1.120
25x6	1.004	1.025	1.097	1.163	1.132	1.106
49x6	1.003	1.023	1.110	1.206	1.179	1.146
98x6	1.004	1.030	1.112	1.171	1.127	1.116
169x6	1.005	1.035	1.134	1.196	1.129	1.141

APRM Channel E

9x6	1.004	1.029	1.111	1.171	1.127	1.118
25x6	1.004	1.025	1.097	1.163	1.130	1.105
49x6	1.003	1.022	1.108	1.205	1.176	1.144
98x6	1.004	1.032	1.116	1.178	1.132	1.121
169x6	1.005	1.037	1.145	1.206	1.136	1.147

APRM Channel F

9x6	1.006	1.034	1.118	1.178	1.133	1.124
25x6	1.005	1.029	1.103	1.169	1.136	1.110
49x6	1.004	1.026	1.117	1.214	1.185	1.152
98x6	1.006	1.038	1.127	1.189	1.143	1.132
169x6	1.009	1.048	1.153	1.217	1.149	1.161

(table con'd.)

APRM Channel G

Nodes	t = 1	t = 2	t = 3	t = 4	t = 5	t = 6
9x6	1.006	1.034	1.118	1.177	1.133	1.123
25x6	1.004	1.028	1.101	1.167	1.135	1.108
49x6	1.004	1.027	1.114	1.212	1.183	1.149
98x6	1.005	1.033	1.116	1.176	1.131	1.121
169x6	1.006	1.038	1.138	1.202	1.136	1.149

APRM Channel H

9x6	1.005	1.033	1.114	1.175	1.131	1.122
25x6	1.004	1.026	1.098	1.166	1.135	1.110
49x6	1.003	1.024	1.109	1.211	1.185	1.153
98x6	1.005	1.032	1.114	1.176	1.133	1.123
169x6	1.005	1.035	1.134	1.198	1.135	1.150

Table 2 - APRM Data for Rod 20-21 Drop

APRM Channel A

Nodes	t = 1	t = 2	t = 3	t = 4	t = 5	t = 6
9x6	1.005	1.032	1.114	1.175	1.132	1.123
25x6	1.006	1.041	1.161	1.236	1.151	1.124
49x6	1.003	1.025	1.119	1.218	1.180	1.146
98x6	1.005	1.039	1.140	1.205	1.154	1.139
169x6	1.006	1.047	1.177	1.248	1.169	1.182

APRM Channel B

9x6	1.005	1.033	1.115	1.174	1.130	1.121
25x6	1.009	1.052	1.161	1.236	1.152	1.127
49x6	1.005	1.032	1.120	1.217	1.181	1.149
98x6	1.009	1.050	1.143	1.204	1.153	1.141
169x6	1.011	1.062	1.186	1.251	1.169	1.181

APRM Channel C

9x6	1.005	1.033	1.114	1.174	1.131	1.122
25x6	1.006	1.038	1.147	1.225	1.145	1.120
49x6	1.003	1.023	1.110	1.208	1.173	1.140
98x6	1.005	1.034	1.122	1.187	1.140	1.129
169x6	1.006	1.043	1.158	1.224	1.149	1.164

APRM Channel D

9x6	1.004	1.029	1.112	1.172	1.129	1.120
25x6	1.005	1.037	1.149	1.231	1.152	1.127
49x6	1.003	1.022	1.111	1.213	1.180	1.149
98x6	1.005	1.035	1.125	1.191	1.144	1.133
169x6	1.006	1.043	1.158	1.225	1.150	1.165

APRM Channel E

9x6	1.004	1.029	1.111	1.170	1.127	1.119
25x6	1.005	1.035	1.141	1.222	1.146	1.122
49x6	1.003	1.021	1.105	1.205	1.171	1.140
98x6	1.005	1.033	1.119	1.187	1.140	1.130
169x6	1.006	1.041	1.152	1.215	1.140	1.155

APRM Channel F

9x6	1.006	1.034	1.118	1.178	1.133	1.124
25x6	1.005	1.036	1.151	1.231	1.152	1.127
49x6	1.003	1.022	1.112	1.212	1.177	1.145
98x6	1.005	1.034	1.132	1.201	1.154	1.143
169x6	1.006	1.042	1.168	1.241	1.168	1.185

(table con'd.)

APRM Channel G

Nodes	t = 1	t = 2	t = 3	t = 4	t = 5	t = 6
9x6	1.005	1.034	1.118	1.177	1.133	1.123
25x6	1.008	1.045	1.160	1.240	1.156	1.128
49x6	1.004	1.028	1.119	1.220	1.184	1.150
98x6	1.006	1.039	1.131	1.198	1.151	1.138
169x6	1.007	1.047	1.166	1.237	1.163	1.179

APRM Channel H

9x6	1.005	1.033	1.114	1.174	1.131	1.122
25x6	1.005	1.037	1.144	1.231	1.156	1.132
49x6	1.003	1.022	1.107	1.211	1.180	1.151
98x6	1.005	1.034	1.122	1.193	1.151	1.143
169x6	1.006	1.042	1.156	1.234	1.165	1.186

INTERPRETATION OF RESULTS

The computed LPRM data depicted on Figures 9 through 18 provides some insight into the effect of varying levels of nodalization on the nuclear instrumentation system. The indicated flux level at each LPRM is calculated by weighing the four nearest nodal fluxes by the distance from the LPRM to the center of those nodes. The 9x6 and 25x6 node cases have multiple LPRMs contained within or on the edge of many nodes. The 49x6, 98x6, and 169x6 node cases have all LPRMs located at the corner of four nodes. This results in equal weighing of the four adjacent nodes for these three cases.

The 169x6 node case can be used as the benchmark for qualitative comparison of the other cases. This case modeled four control cells in each node surrounding the LPRM. The flux computed in those nodes is used in calculating the indication for no more than one LPRM. The two major peaks are produced principally from the LPRMs strings nearest to the control rod being dropped. As the control rod is withdrawn from a core region, the absorbtion of neutrons in the control rod decreases which increases the local flux in that node and the leakage flux into the adjacent nodes. The shape of the LPRM flux is almost purely representative of the nodal flux shape.

The 98x6 and 49x6 node cases each have pairs of identical shape and size peaks. Each node in the 98x6 case

is composed of two control cells and a single node may be adjacent to two LPRMs. Each node in the 49x6 case is composed of four control cells and a single node may be adjacent to four LPRMs. This results in an indication of a broader flux peak than is actually occurring.

The 25x6 node case has as many as nine control cells within each node with as many as four LPRMs inside or on the edge of each node. The indicated flux on each of those LPRMs is dominated by the flux in that node but has a weighted contribution from the other three adjacent nodes nearest to the LPRM. This results in two major flux peaks similar to the 169x6 node case in shape for the rod 28-29 case but of a lower magnitude. The rod 20-21 case has two nearly identical peaks due to the location of the control rod being directly between two LPRMs.

The 9x6 node case has as many as twenty-five control cells within each node and as many as nine LPRMs within or on the edge of each node. This case indicated some peaking during the control rod drop but the large node volumes had the effect of smearing the flux peak over multiple LPRMs. The definition of the local effect was all but lost.

CONCLUSIONS AND RECOMMENDATIONS

The quantitative comparison between the different levels of nodalization must be made based on the APRM response to the two control rod drop events. For the dropping of control rod 28-29, the 9x6, 49x6, 98x6, and 169x6 node configurations each would have produced a reactor trip signal. The 25x6 configuration would not have produced a trip. For the dropping of control rod 20-21, each of the nodal configurations would have produced a reactor trip.

A qualitative comparison of the LPRM data for each nodal configuration can be performed. The most distinct representation of flux on the LPRMs is produced from the 169x6 node case. Each LPRM is calculated from a unique set of adjacent nodal fluxes. The weighing of nodal fluxes in the 25x6, 49x6 and 98x6 cases tend to indicate a broader and flatter flux peak than is actually being calculated in the model. The 9x6 node case produces minimal peaking with poor definition due to the large node volumes.

The data indicates that each level of nodalization except the 25x6 level is acceptable from the regulatory standpoint based on the quantitative comparison. The variation from the qualitative comparison of the LPRM data for the each case except the 9x6 level is relatively minor. The area of the flux peak for the 25x6, 49x6, and 98x6

cases are smaller in amplitude and wider than the 169x6 case but a distinct peak is evident. The intent of indicating a flux peak and producing a reactor trip is met in each of the cases above the 25x6 level. The computer memory and time requirements for each level of nodalization varies linearly with the number of nodes, making the lowest level of nodalization most attractive from a cost standpoint.

The level of nodalization that provides four nodes adjacent to each location of internal flux level measurement appears to be adequate for real time simulation applications to be used for operator training. The 49x6 node configuration was the minimum configuration studied that meets that requirement. The levels of nodalization that rely on distance weighted flux levels to provide the input to the nuclear instrumentation, such as the 9x6 and 25x6 cases studied here, do not provide fine enough detail for very localized events such as a control rod drop. These cases may be suitable for more global events but care would have to be taken to ensure that localized effects were not studied.

REFERENCES

American Nuclear Society, 1985. ANSI/ANS-3.5-1985 Nuclear Power Plant Simulators for Use in Operator Training. La Grange Park, Ill.: American Nuclear Society.

Delp, D.L., D.L. Fisher, J.M. Harriman, and M.J. Stedwell, 1964. FLARE, a three-dimensional boiling water reactor simulator. San Jose: General Electric Atomic Power Equipment Department, GEAP-4598.

Gonsalves,J.B. and J.E. Proctor 1987. Nuclear plant simulators: the past and the present. Nuclear News (June): 49-55.

Gulf States Utilities Company 1987. River Bend Station Updated Safety Analysis Report, Amendment 35. Beaumont, Tx.: Gulf States Utilities Company.

Henry, Allan F., 1986. Nuclear-reactor analysis. Cambridge, Mass.: The MIT Press.

Kazimi, Mujid S. and Neil E. Todreas, 1989. Nuclear Systems I. New York: Hemisphere Publishing Corp.

VITA

Charles Austin Rohrmann was born in Queens Village, New York, September 29, 1953. He has lived in many areas of the United States including California, Idaho, Virginia, and Louisiana. He graduated from North High School in Torrance, California, June 1971. He attended Central Virginia Community College in Lynchburg, Virginia receiving an Associate of Science in Engineering in June 1983. He attended Louisiana State University in Baton Rouge, Louisiana receiving a Bachelor of Science in Mechanical Engineering in December 1989.

He served for eight years in the U.S. Navy in the areas of chemistry, health physics, and operations of naval reactors. He spent four years as a simulator instructor with the Babcock and Wilcox Company and has supervised the operation and maintenance of the River Bend Station simulator for eleven years.

In March, 1992, he began to pursue his Masters of Science in Nuclear Engineering at Louisiana State University and is a candidate for that degree.